Physics and Imaging in Radiation Oncology 32 (2024) 100638

Contents lists available at ScienceDirect

Physics and Imaging in Radiation Oncology

journal homepage: www.sciencedirect.com/journal/physics-and-imaging-in-radiation-oncology

Original Research Article

In vivo dosimetry with an inorganic scintillation detector during multi-channel vaginal cylinder pulsed dose-rate brachytherapy: Dosimetry for pulsed dose-rate brachytherapy

Peter D. Georgi [a,*], Søren K. Nielsen [b], Anders T. Hansen [b], Harald Spejlborg [b], Susanne Rylander [b], Jacob Lindegaard [b], Simon Buus [b], Christian Wulff [a], Primoz Petric [b], Kari Tanderup [a,b], Jacob G. Johansen [a,b]

[a] Department of Clinical Medicine, Aarhus University, Aarhus, Denmark
[b] Department of Oncology, Aarhus University Hospital, Aarhus, Denmark

ARTICLE INFO

Keywords:
Time-resolved in vivo dosimetry
Pulsed dose-rate brachytherapy
Inorganic scintillator

ABSTRACT

Background and purpose: In vivo dosimetry is not standard in brachytherapy and some errors go undetected. The aim of this study was to evaluate the accuracy of multi-channel vaginal cylinder pulsed dose-rate brachytherapy using in vivo dosimetry.
Materials and methods: In vivo dosimetry data was collected during the years 2019–2022 for 22 patients (32 fractions) receiving multi-channel cylinder pulsed dose-rate brachytherapy. An inorganic scintillation detector was inserted in a cylinder channel. Each fraction was analysed as independent data sets. In vivo dosimetry-based source-tracking was used to determine the relative source-to-detector position. Measured dose was compared to planned and re-calculated source-tracking based doses. Assuming no change in organ and applicator geometry throughout treatment, the planned and source-tracking based dose distributions were compared in select volumes via γ-index analysis and dose-volume-histograms.
Results: The mean ± SD planned vs. measured dose deviations in the first pulse were 0.8 ± 5.9 %. In 31/32 fractions the deviation was within the combined in vivo dosimetry uncertainty (averaging 9.7 %, $k = 2$) and planning dose calculation uncertainty (1.6 %, $k = 2$). The dwell-position offsets were < 2 mm for 88 % of channels, with the largest being 5.1 mm (4.0 mm uncertainty, $k = 2$). 3 %/2 mm γ pass-rates averaged 97.0 % (clinical target volume (CTV)), 100.0 % (rectum), 99.9 % (bladder). The mean ± SD deviation was −1.1 ± 2.9 % for CTV D98, and −0.2 ± 0.9 % and −1.2 ± 2.5 %, for bladder and rectum D2cm^3 respectively, indicating good agreement between intended and delivered dose.
Conclusions: In vivo dosimetry verified accurate and stable dose delivery in multi-channel vaginal cylinder based pulsed dose-rate brachytherapy.

1. Introduction

Image guided brachytherapy is essential for gynaecological cancer radiotherapy enabling highly conformal dose-plans [1–5]. Compared to high dose-rate (HDR) brachytherapy, pulsed dose-rate (PDR) brachytherapy potentially exhibits superior radiobiological effect and optimisation through tissue repair kinetics [6–10]. However, PDR brachytherapy is a complex procedure, often delivered as hourly pulses over a > 20-hour period, increasing risks of errors.

Multi-channel vaginal cylinder (MVC) applicators are suited for specific diseases. Its rigidness warrants accurate dose delivery. However, processes within brachytherapy could cause source position offsets, including erroneous applicator registration and wrongly connected guide-tubes, with adverse consequences [11–13]. Such errors are likely underreported [14], and the clinical detriment difficult to estimate.

In vivo dosimetry (IVD) studies have shown dose offsets of 37 % in gynaecological brachytherapy [14–19] attributed to suboptimal detector positioning. Two studies utilized time-resolved dosimetry capable of detecting errors not resolved by accumulated dose measurements [20]. Tanderup et al. used diode arrays [19], while Belley et al. used fiber-

* Corresponding author at: Department of Clinical Medicine, Aarhus University, Palle Juul-Jensens Boulevard 82, DK-8200 Aarhus N, Denmark.
E-mail address: pegeor@clin.au.dk (P.D. Georgi).

https://doi.org/10.1016/j.phro.2024.100638
Received 31 January 2024; Received in revised form 21 August 2024; Accepted 22 August 2024
Available online 25 August 2024

coupled inorganic scintillation detectors Tanderup et al. exploited the temporal information for geometric validation but measured dose in the rectum. Belley et al. measured the dose within target areas, but did no geometric validation [18]. Hence, in contrast to prostate cancer brachytherapy [20–24], in-target IVD-based geometric validation target has not been performed for gynecological brachytherapy.

The aim of this study was to investigate the dosimetric accuracy of image-guided MVC-based PDR brachytherapy using time-resolved IVD with an inorganic scintillation detector, and quantify the effect of dwell-position instabilities on clinical parameters such as dose volume histograms (DVH) and γ-index pass-rates.

2. Materials and methods

IVD data was obtained from 24 patients (48 fractions) treated with MVC PDR brachytherapy for gynaecological cancer between January 2019 and September 2022 at Aarhus University Hospital. Based on nine inclusion criteria, 22 patients (32 fractions) were selected for analysis (Supplementary Material S1). Each fraction included applicator insertion and treatment planning independent from previous fractions. Hence, each fraction was considered an independent treatment.

2.1. Patients and treatment

Patients were treated with external beam radiotherapy followed by two fractions of magnetic resonance image-guided PDR brachytherapy (20 hourly pulses). Dose delivery was optimised for equivalent dose at 2 Gy per fraction [25,26]. The cumulative dose was 45 Gy in 25 fractions for external beam radiotherapy and 30 Gy in two fractions for brachytherapy. Radiation was delivered with a GammaMed PDR ^{192}Ir Plus source (Varian Medical Systems, US). The applicators were plastic MVCs with 1.2 mm diameter channels through the centre and along the periphery (Fig. 1a). The central to outer channel distances were 11 mm (in-house made), 12.5 mm, and 15 mm (Varian Medical Systems, US). Treatment planning was performed using Brachyvision (Varian Medical Systems, US).

2.2. In vivo dosimetry and data collection

IVD was performed with an in-house developed inorganic scintillation detector as a part of the clinical protocol. The sensitive volume was a ZnSe:O crystal (0.5 × 0.5 × 1.0 mm^3, ISMA, Ukraine) coupled to a photodetector (S8746-01Si-diode, Hamamatsu, Japan) via an optical fibre (Ø: 0.5 mm, GH-2001-P, Eska Mitsubishi Rayon Co., Japan) (Fig. 1b). The photodetector signal was recorded in Volts (at 20 Hz rate) via a data acquisition device (USB2408, Measurement Computing, UK), and a single-board computer (Raspberry Pi v3.0, Raspberry Pi Ltd., UK).

Before each treatment, the detector was calibrated with a previously described method [27]. A spare MVC channel was chosen to house the detector. After guide-tube connection, the detector probe was put in this channel and fixed with a locking mechanism to ensure positional stability. The distance between the detector tip and locking mechanism was used as the distance between the marked detector position and channel entrance in the treatment plan. If the probe detached from the MVC (primarily due to large patient movements), the IVD procedure was stopped. Thus, some fraction measurements constitute less than 20 pulses.

2.3. Data analysis

The data was anonymised and analysed post-treatment in accordance with the obtained approval to use the data. The measured signal was segmented into three levels of detail: pulses, channels, and dwells (Fig. 2). The dose-rate for each dwell-position was determined using eq. (2.1) adopted from other studies [28,29],

$$\dot{D}^{meas}_{w,Q,i}(z_i, x_i, z_{det}, x_{det}) = N_{D,w,Q_0} \cdot k_{Q,Q_0}(z_i, x_i, z_{det}, x_{det}) \cdot M_{meas,i} \tag{2.1}$$

'i' represents the dwell-position number and 'det' the detector position. M_{meas} is the mean measured signal at each dwell-position (Fig. 2d, only innermost 90 % to exclude edge-effects). N_{D,w,Q_0} is the calibration factor. $k_{Q,Q_0}(z,x)$ is a position dependent radiation quality correction factor [27,30,31].

A study showed that the dwell-time during delivery matches with the treatment plan dwell-times within 0.15 s [22]. Hence, the measured dose for each dwell-position was calculated by multiplying the measured dose-rate with the planned dwell-times. The measured dose at the detector position (henceforth referred to as detector dose) per pulse was calculated as the contribution from all dwell-positions. The fractional detector dose was calculated by summing the individual pulse contributions.

The detector mark in the treatment plan was found to be imprecise. The detector position was therefore determined based on the IVD data via source-tracking as in previous studies [23,32]. For each pulse the detector position within its channel was updated to its most likely position based on the measured signal, using cylindrical coordinates (Fig. 3a). The z-axis was defined as the long axis of the MVC originating at the detector sensitive volume. The x-axis was the radial distance between the detector and source channels (Fig. 3a). The most likely relative detector-to-dwell positions were determined as the coordinates (z',x') minimising

$$\sum_{(z,x)} \left[\frac{f_M(z',x',N_{D,w,Q_0}) - M_{meas}(z',x')}{\sigma_{M(z',x')}} \right]^2, \tag{2.2}$$

with $M_{meas}(z',x')$ and $\sigma_{M(z',x')}$ being the measured mean and one standard deviation (SD) of the signal for a given dwell-position respectively (Fig. 2d), and $f_M(z',x')$ being a function providing the expected signal at

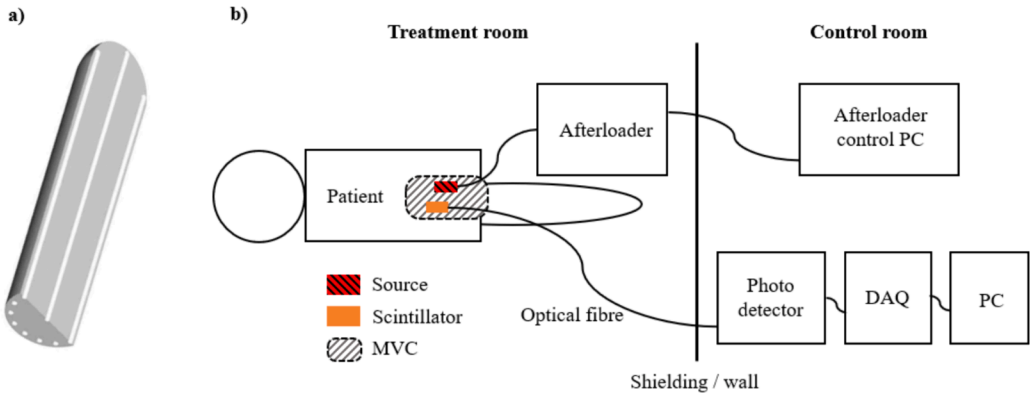

Fig. 1. a) Cross-section of an MVC applicator. b) PDR brachytherapy and in vivo dosimetry setup. PDR.

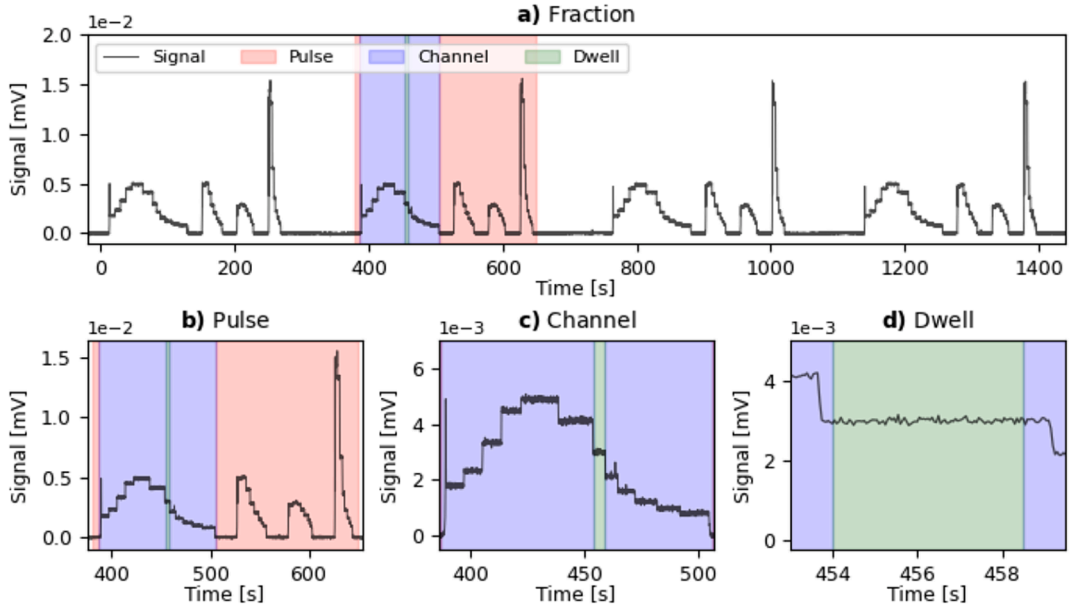

Fig. 2. a) Example of the raw IVD signal from a PDR brachytherapy treatment. Zoom-ins of the signal are presented for a b) pulse, c) channel, and d) dwell-position.

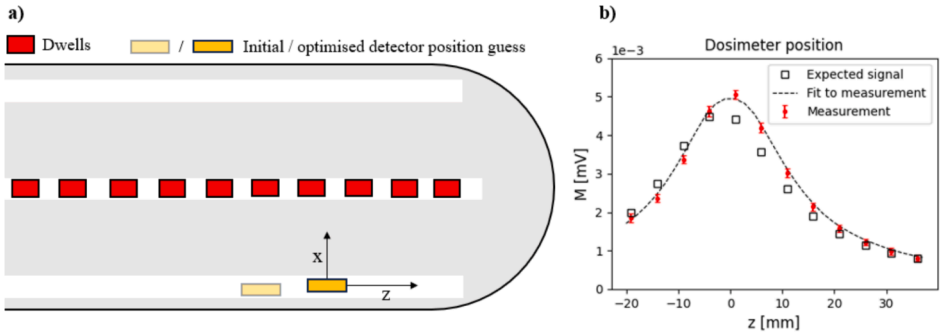

Fig. 3. a) Example sketch of detector- and dwell-positions within a MVC showing, the detector position marked in the treatment plan (transparent orange) and after measurement-based fit (solid orange). b) b) Detector position optimisation example showing the expected (squares) and measured (dots) signal vs position and fit (dashed line) to the data. (For interpretation of the references to colour in this figure legend, the reader is referred to the web version of this article.)

(z', x'),

$$f_M(z', x', N_{D,w,Q_0}) = \frac{\dot{D}_{w,TG43}(z', x')}{N_{D,w,Q_0} \cdot k_{Q,Q_0}(z', x')}. \quad (2.3)$$

$\dot{D}_{w,TG43}$ is the TG-43 dose-rate [33]. The source and detector's longitudinal axes were assumed parallel. The longitudinal inter-dwell-distances (source stepping length) were assumed to be delivered as planned (Fig. 3a–b). Only channels with ≥ 4 dwells were used to ensure robust source-tracking [32]. Two sets of relative source-to-dwell positions were defined, the *planned* and *tracked* set. For the planned set, the x-coordinates were defined as the radial distances between the detector and dwell-positions dictated by the MVC geometry, while the z-coordinates were defined as the mean of the tracked most likely detector z-position in all channels. For the tracked set, the most likely x-coordinates based on measurements were used, enabling validation of MVC delineation, and the z-coordinates were defined as most likely detector z-coordinate based on measurements for each individual channel relative to the mean z-coordinate in the planned set.

Source-tracking was performed for 154/192 channels (supplementary material S1). The detector dose was calculated for the two sets of detector-to-dwell positions and compared to the measurements. The tracking uncertainty was based on the source-tracking algorithm and calibration uncertainty [31,32]. The most accurate tracking (<1 mm uncertainty, $k = 2$) was reached if dwell-positions spanned across the x-axis relative to the source (Fig. 3a), while the number of dwell-positions had negligible effect.

The temporal geometric stability of all treatments was evaluated by comparing the measured dose and positions across pulses.

Dosimetric stability was considered for the clinical target volume (CTV), rectum, and bladder. The volume of interest (VOI) geometries and position relative to the MVC were based on plan delineations. Hence, potential anatomical changes including shift of the MVC relative to anatomy was unaccounted for. This was considered the best option, to include anatomical information not obtained with IVD, but is a limitation of the study. The VOIs were chosen to investigate measured effects in patient geometries and minimize clinically irrelevant dose discrepancies. The VOI dose distributions for the planned and tracked dwell-positions were calculated for all fractions and pulses in 1 mm^3 voxels. Only longitudinal dwell-position shifts were included since, due to the MVC rigidness, radial shifts were primarily ascribed to methodology uncertainties. γ-index pass-rate analysis (henceforth γ-analysis) was performed for each fraction and pulse. 23 CTVs (27 bladders and rectums) were included (supplementary material S1). γ-analysis was performed with a global 3 %/2 mm pass criteria, excluding doses below 10 % of prescribed dose, as recommended for intensity modulated radiotherapy (IMRT) by the American Association of Physicists in Medicine [34].

Offsets in D98 of the CTV and D2cm^3 of the rectum and bladder were calculated for the first pulse.

3. Results

3.1. Comparison with treatment plan

The measured and calculated dose (first pulse) agreed within the combined, $k = 2$, uncertainties of the measurements (averaging 9.7 %) and planned dose (~1.6 %) for 31/32 fractions (Fig. 4a). The mean ± SD of the planned-measured detector dose across all fractions and pulses was 0.8 ± 5.9 % (Fig. 4e). Correcting for the tracked positional off-sets reduced the mean ± SD of the deviation between measured and calculated dose to 0.1 ± 1.0 % (Fig. 4a and e). No correlation was observed between fractions within the same patient.

The tracked positions agreed with the treatment plan within the IVD uncertainties ($k = 2$) for 149/154 catheters considering both directions (Fig. 4b–c). The largest tracked offset (first pulse) for a channel was radially −3.5 mm (tracking uncertainty: 3.9 mm, $k = 2$) and longitudinally −4.3 mm (tracking uncertainty: 0.5 mm, $k = 2$). Across all fractions and pulses the mean ± SD of the offsets were −0.1 ± 1.1 mm radially and 0.0 ± 1.1 mm longitudinally (Fig. 4f–g). Offsets < 2(>3) mm were observed in 92.4(0.6)% (radial) and 94.4(2.0)% (longitudinal) of channels across all pulses. The largest offset was 5.1 mm longitudinally (tracking uncertainty: 4.0 mm, $k = 2$).

The mean of the γ-index pass-rates were 97.0 % (CTV), 100.0 % (rectum), 99.9 % (bladder). Five fractions had pass-rates below 95 % in the CTV for the first pulse. Two of these fractions had pass-rates below 90 % (Fig. 4d).

The overall mean ± SD of the deviation between planned and recalculated (based on source-tracking) CTV D98 was −0.2 ± 0.4 Gy (−1.1 ± 2.9 %). For the rectum and bladder D2cm^3 it was −0.0 ± 0.1 Gy (−0.2 ± 0.9 %) and −0.1 ± 0.2 Gy (−1.2 ± 2.5 %) respectively. The largest offset of CTV D98 during the first pulse was −15.2 % (Fig. 4d). The largest offsets for D2cm^3 in the rectum and bladder were −2.9 %and −11.7 %respectively.

3.2. Pulse-to-pulse variation

The deviation between measured dose in the first pulse relative to the subsequent pulses changed from a mean ± SD of −0.1 ± 0.8 % (pulse 2) to 0.6 ± 3.5 % (pulse 20) (Fig. 5a). The radial offsets relative to the first pulse increased across all fractions from a mean ± SD of 0.0 ± 0.3 mm (pulse 2) to 0.0 ± 0.7 mm (pulse 20) (Fig. 5b). The values for the longitudinal offsets were 0.0 ± 0.7 mm (pulse 2) to 0.0 ± 1.0 mm (pulse 20) (Fig. 5b). The increasing SD of the positional offsets were mainly dominated by inter-fraction variations. Individual fractions generally fluctuated less than indicated by the presented SD but could systematically shift with increasing pulse number.

4. Discussion

Analysis of time-resolved IVD data during 32 MVC-based PDR brachytherapy fractions indicated good agreement between planned and delivered dose and treatment geometry in terms of relative dwell-positions, with high stability throughout the entire treatment.

The deviations between the planned and measured dose ranged from −15 to + 15 % with an SD of 5.9 % ($k = 1$). This is in good agreement with previous IVD studies on gynaecological brachytherapy, which reported SD in the range of 5–9 % [14–19]. The geometric precision found in this study was also similar to the ~2 mm applicator-diode distance reported by Tanderup et al. [19]. The deviation in dose and dwell-positions could be largely explained by uncertainties related to image-based applicator reconstruction and detector position. In this study, the measured detector dose was stable during the entire treatment, with a small increase in the SD (from 0.8 % to 3.5 %) of measured dose relative to the first pulse as function of pulse number (Fig. 5a). This coincides with the 5 % found by Tanderup et al. [19] Thus, measurements suggested that treatment was delivered as planned during the first pulse and stayed stable throughout treatment.

For the CTV a high concordance between planned and recalculated dose distribution was observed with a mean γ-index pass-rate of 97.0 %. For source quality assurance in IMRT, the American Association of Physicists in Medicine recommends a 95 % tolerance and 90 % action level limit [34]. With those limits, 3/23 fractions would not fulfil the tolerance criterion, while two treatments would not fulfil the action criterion (Fig. 4d). However, dose distribution in IMRT quality assurance is much more homogeneous, and highly controlled. Thus, these tolerance limits might be too strict for brachytherapy. Two HDR brachytherapy phantom studies reported a pass-rate of 95.9 % (1 %/1 mm pass criterion for the area with > 50 % of prescribed dose) [35] and > 99.8 % (3 %/3 mm pass criterion) [36] respectively. This indicates that pass-rates like those in IMRT might be expected in brachytherapy, though these examples are likely not representative of in vivo γ-analysis. While this study cannot provide tolerances for γ-index pass-rates, especially considering the assumption of a stable anatomy, it provides an initial estimate of what values might be expected in PDR brachytherapy. The pass-rates in the rectum and bladder were all larger than 98 %. The high pass-rates indicate that planned tumour coverage and sparing of organs at risk are robust towards positional shifts of the source of the magnitudes measured in this study. A former study on catheter-based HDR brachytherapy for prostate cancer, indicated that a 3 mm displacement of a catheter could lead to 5 % dose change in the prostate gland [37]. Only 3/154 channels in this study had displacements of that magnitude, potentially explaining the high pass-rates. Thus, the observed displacements likely have limited clinical relevance.

The fraction with the lowest γ-index pass-rate in the CTV, had the largest change in the CTV D98 (patient 5, fraction 1, $\gamma = 74.1$ %, Δ D98 = -15.2 %). Its largest positional offset of a channel was 2.0 ± 0.8 mm ($k = 2$), smaller than those reported for significant dosimetric change in prostate treatments [37]. However, for this treatment, a longitudinal shift of the channels would move dwell-positions directly towards/away from a significant portion of the CTV (Fig. S2a), making its dose coverage sensitive to positional displacements. Patient 12, fraction 1, showed the second smallest γ-index pass-rate (87.2 %), but a smaller change in CTV D98 (−3.5 %), despite a larger longitudinal offset of a channel (4.0 ± 4.0 mm, $k = 2$). The reason might be less sensitivity to longitudinal offsets, since here they would not move dwell-positions directly towards/away from any part of the CTV (Fig. S2b). Similarly, Jørgensen et al. [23] observed that some catheter shifts in prostate HDR brachytherapy of >1 cm did not cause clinically relevant changes to DVH parameters in some patient geometries. Thus, poor γ-index pass-rates do not necessarily correspond to worse dose coverage suggesting that accuracy requirements could be plan specific.

Limitations of this study are the lack of independent calibration and absolute positional information relative to patient anatomy. Independent calibration is necessary to detect source calibration or source strength errors. Additionally, if the MVC applicator is displaced, the detector will follow. Thus, it can only provide information on the relative geometry within the MVC. Positional changes in relation to the patient anatomy are not resolved, and the accuracy of the DVH parameter and γ-index pass-rate is unknown. A possible solution could be to combine the detector with imaging panels that have shown potential for anatomical imaging, utilising the brachytherapy radiation [35]. However, the IVD system allows detection of other errors, such as channel swaps, wrong guide-tube lengths, and dwell-time errors [14,20].

Source-tracking was applicable to 80 % of channels. The impact of non-tracked channels on the analysis depends on their dwell-times and proximity to VOIs. In this study 27/32 fractions had <10 % contribution to the total dwell-time from channels with less than four dwells (Fig. S3). If their distance to VOIs is relatively large, positional errors have limited

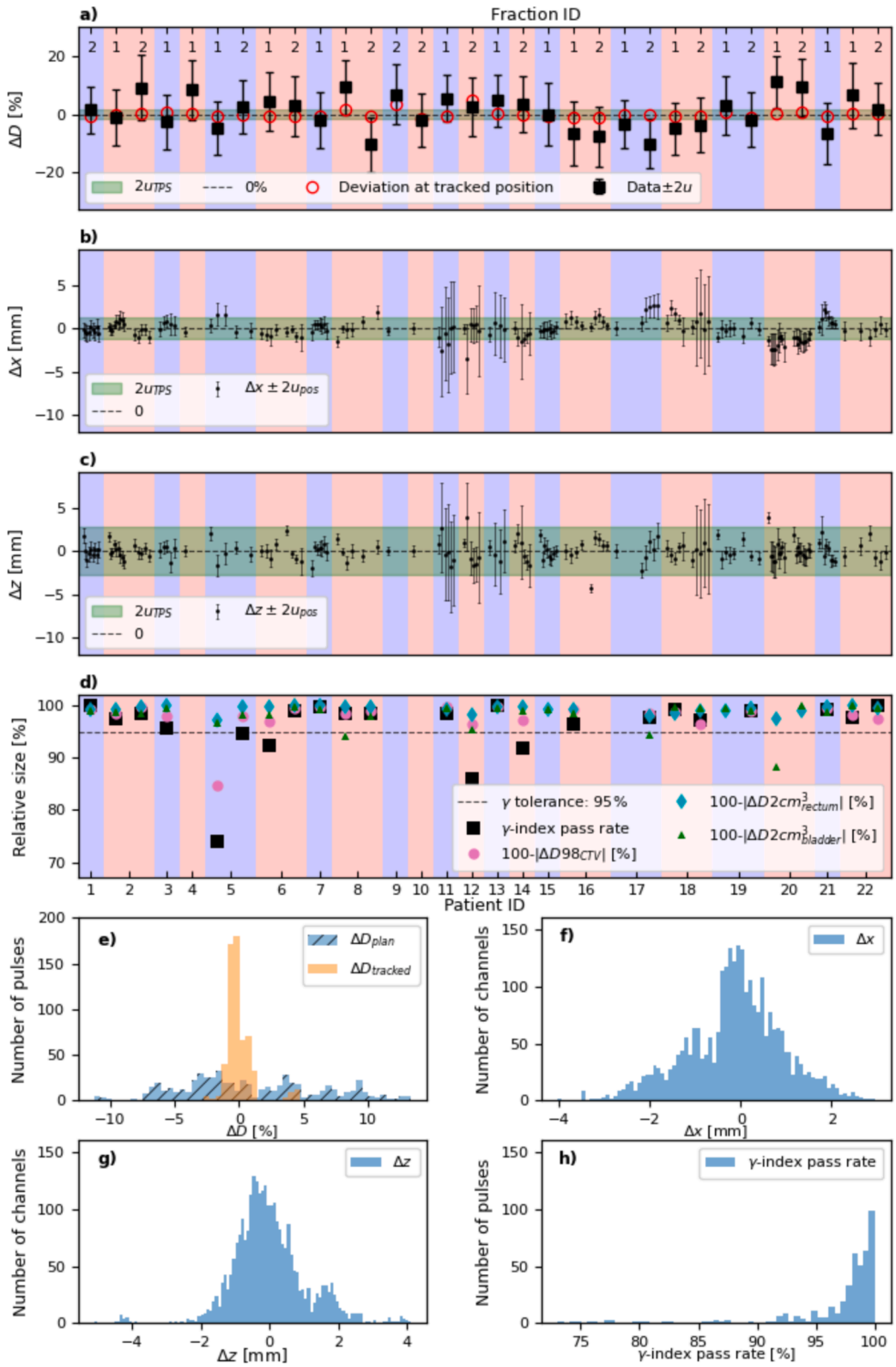

Fig. 4. a) Deviation between planned and measured dose at the detector position for the individual entire treatment fractions for the planned (squares) and tracked (circles) dwell-positions. b–c) Radial and longitudinal deviations between planned and tracked channel positions for the first pulse of each treatment fraction. The treatment planning software uncertainty (U_{TPS}) is shown as a band in figure a–c. d) Global 3 %/2 mm γ-index pass-rate for each fraction for the first pulse (squares) and relative off-set of D98 in the CTV (circles), and D2cm^3 in the rectum (diamonds) and bladder (triangles). e) Deviation between measured and calculated dose per pulse at the detector position for the planned (hatched) and tracked (solid) dwell-positions. f–g) All deviations between planned and tracked radial (x) and longitudinal (z) positions of channels. h) Distribution of global 3 %/2 mm γ-index pass-rate for all pulses within the CTV, bladder, and rectum.

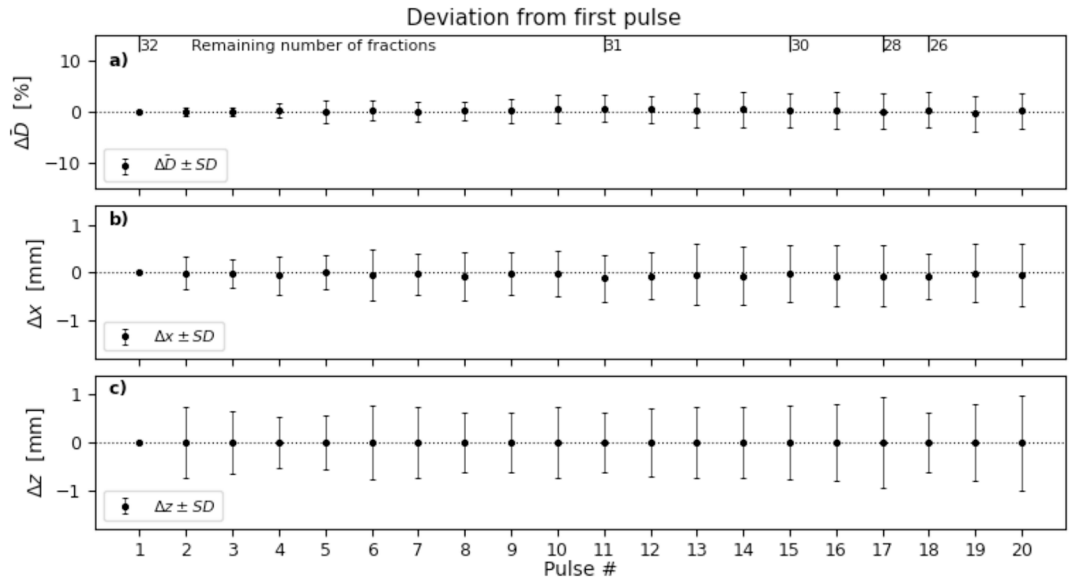

Fig. 5. a) The mean ± SD deviation between measured dose relative to the first pulse across all fractions. b–c) The mean ± SD deviation between tracked channel radial (b) and longitudinal (c) position relative to the first pulse across all channels of all fractions. The longitudinal displacements are relative to the mean tracked position.

clinical impact, though short distances might warrant concern. For 5/32 fractions the channels with four or less dwell-positions constituted a major fraction of the total dwell-time, though these were not included in the DVHs and γ-analysis since they only had source-tracking performed for a single channel. The agreement between measured and planned detector dose indicates that these channels did not cause large discrepancies, but future studies should include their uncertainty contribution.

In conclusion, the IVD method validated the relative geometry and dose distribution of PDR brachytherapy, showing good agreement between plan and delivery. Potentially, clinics can use the combined information of the intended treatment and IVD information to address positional and dosimetric offsets.

CRediT authorship contribution statement

Peter D. Georgi: Conceptualization, Methodology, Software, Validation, Formal analysis, Investigation, Data curation, Writing – original draft, Writing – review & editing, Visualization, Project administration. **Søren K. Nielsen:** Validation, Investigation, Writing – review & editing. **Anders T. Hansen:** Investigation, Writing – review & editing. **Harald Spejlborg:** Investigation, Writing – review & editing. **Susanne Rylander:** Investigation, Writing – review & editing. **Jacob Lindegaard:** Validation, Investigation, Writing – review & editing. **Simon Buus:** Validation, Investigation, Writing – review & editing. **Christian Wulff:** Validation, Investigation, Writing – review & editing. **Primoz Petric:** Validation, Investigation, Writing – review & editing. **Kari Tanderup:** Conceptualization, Resources, Writing – review & editing, Supervision, Project administration, Funding acquisition. **Jacob G. Johansen:** Conceptualization, Methodology, Software, Validation, Investigation, Resources, Data curation, Writing – review & editing, Supervision, Project administration, Funding acquisition.

Declaration of competing interest

The authors declare the following financial interests/personal relationships which may be considered as potential competing interests: While these relations have had no influence on the findings of this work, the authors find it appropriate to inform on the following financial and advisory connections: The study has been funded by: - Aarhus University open access agreement (granted to all Aarhus University affiliated research). - Novo Nordisk Fonden (for the research group and not specifically for this study). Author-specific relations: Jacob G Johansen: - Research collaboration with ELEKTA (not this study). - Member of ORIGIN (https://origin2020.eu/) advisory board. - Member of BRAPHYS work-group under GEC-ESTRO. - No-voting consultant in AAPM Working Group on Medical Errors in brachytherapy (WGMEB). Kari Tanderup: - Grant from Danish Cancer Society (not specifically for this study). Research collaboration with ELEKTA (not this study). The remaining authors have not relations of interest.

Acknowledgements

This study was funded via Novo Nordisk Fonden grant NNF19OC0058756.

Appendix A. Supplementary data

Supplementary data to this article can be found online at https://doi.org/10.1016/j.phro.2024.100638.

References

[1] Williams VM, Kahn JM, Thaker NG, Beriwal S, Nguyen PL, Arthur D, et al. The case for brachytherapy: why it deserves a renaissance. Adv Radiat Oncol 2020;6:100605. https://doi.org/10.1016/j.adro.2020.10.018.
[2] Tanderup K, Eifel PJ, Yashar CM, Pötter R, Grigsby PW. Curative radiation therapy for locally advanced cervical cancer: brachytherapy is NOT optional. Int J Radiat Oncol 2014;88:537–9. https://doi.org/10.1016/j.ijrobp.2013.11.011.
[3] Han K, Milosevic M, Fyles A, Pintilie M, Viswanathan AN. Trends in the utilization of brachytherapy in cervical cancer in the United States. Int J Radiat Oncol 2013;87:111–9. https://doi.org/10.1016/j.ijrobp.2013.05.033.
[4] Pötter R, Tanderup K, Schmid MP, Jürgenliemk-Schulz I, Haie-Meder C, Fokdal LU, et al. MRI-guided adaptive brachytherapy in locally advanced cervical cancer (EMBRACE-I): a multicentre prospective cohort study. Lancet Oncol 2021;22:538–47. https://doi.org/10.1016/S1470-2045(20)30753-1.
[5] Karlsson J, Dreifaldt A-C, Bohr Mordhorst L, Sorbe B. Differences in outcome for cervical cancer patients treated with or without brachytherapy. Brachytherapy 2017;16:133–40. https://doi.org/10.1016/j.brachy.2016.09.011.
[6] Brenner DJ, Hall EJ. Conditions for the equivalence of continuous to pulsed low dose rate brachytherapy. Int J Radiat Oncol Biol Phys 1991;20:181–90. https://doi.org/10.1016/0360-3016(91)90158-Z.
[7] Mason KA, Thames HD, Ochran TG, Ruifrok ACC, Janjan N. Comparison of continuous and pulsed low dose rate brachytherapy: biological equivalence *in vivo*. Int J Radiat Oncol 1994;28:667–71. https://doi.org/10.1016/0360-3016(94)90192-9.

[8] Couto JG, Bravo I, Pirraco R. Biological equivalence between LDR and PDR in cervical cancer: multifactor analysis using the linear-quadratic model. J Contemp Brachytherapy 2011;3:134. https://doi.org/10.5114/jcb.2011.24820.
[9] Balgobind BV, Koedooder K, Ordoñez Zúñiga D, Dávila Fajardo R, Rasch CRN, Pieters BR. A review of the clinical experience in pulsed dose rate brachytherapy. Br J Radiol 2015;88:20150310. https://doi.org/10.1259/bjr.20150310.
[10] Skowronek J. Pulsed dose rate brachytherapy – is it the right way? J Contemp Brachytherapy 2010;2:107–13. https://doi.org/10.5114/jcb.2010.16921.
[11] International Commission on Radiological Protection. Prevention of high-dose-rate brachytherapy accidents. Ann ICRP 2005;35. https://doi.org/10.1016/j.icrp.2005.05.001.
[12] UK Health Security Agency. Safer radiotherapy: biennial error analysis and learning. GOVUK 2022. https://www.gov.uk/government/publications/radiotherapy-errors-and-near-misses-data-report (accessed September 19, 2023).
[13] Public Health England. Radiotherapy error and near-miss data report: December 2015 to November 2017 2015. https://webarchive.nationalarchives.gov.uk/ukgwa/20221101150222/https://www.gov.uk/government/publications/radiotherapy-errors-and-near-misses-data-report (accessed May 30, 2022).
[14] Fonseca GP, Johansen JG, Smith RL, Beaulieu L, Beddar S, Kertzscher G, et al. In vivo dosimetry in brachytherapy: requirements and future directions for research, development, and clinical practice. Phys Imaging Radiat Oncol 2020;16:1–11. https://doi.org/10.1016/j.phro.2020.09.002.
[15] Gellekom MPRV, Canters RAM, Dankers FJWM, Loopstra A, van der Steen-Banasik EM, Haverkort MAD. In vivo dosimetry in gynecological applications—a feasibility study. Brachytherapy 2018;17:146–53. https://doi.org/10.1016/j.brachy.2017.04.240.
[16] Carrara M, Romanyukha A, Tenconi C, Mazzeo D, Cerrotta A, Borroni M, et al. Clinical application of MOSkin dosimeters to rectal wall in vivo dosimetry in gynecological HDR brachytherapy. Phys Med 2017;41:5–12. https://doi.org/10.1016/j.ejmp.2017.05.003.
[17] Jamalludin Z, Jong WL, Malik RA, Rosenfeld AB, Ung NM. Evaluation of rectal dose discrepancies between planned and in vivo dosimetry using MOSkin detector and PTW 9112 semiconductor probe during 60Co HDR CT-based intracavitary cervix brachytherapy. Phys Med 2020;69:52–60. https://doi.org/10.1016/j.ejmp.2019.11.025.
[18] Belley MD, Craciunescu O, Chang Z, Langloss BW, Stanton IN, Yoshizumi TT, et al. Real-time dose-rate monitoring with gynecologic brachytherapy: results of an initial clinical trial. Brachytherapy 2018;17:1023–9. https://doi.org/10.1016/j.brachy.2018.07.014.
[19] Tanderup K, Christensen JJ, Granfeldt J, Lindegaard JC. Geometric stability of intracavitary pulsed dose rate brachytherapy monitored by in vivo rectal dosimetry. Radiother Oncol 2006;79:87–93. https://doi.org/10.1016/j.radonc.2006.02.016.
[20] Kertzscher G, Andersen CE, Tanderup K. Adaptive error detection for HDR/PDR brachytherapy: guidance for decision making during real-time in vivo point dosimetry. Med Phys 2014;41:052102. https://doi.org/10.1118/1.4870438.
[21] Graversen Johansen J, Rylander S, Buus S, Bentzen L, Hokland SB, Skou Søndergaard C, et al. Time-resolved in vivo dosimetry for source tracking in brachytherapy. Brachytherapy 2018;17:122–32.
[22] Johansen J, Kertzscher G, Jørgensen EB, Rylander S, Bentzen L, Hokland SB, et al. Dwell time verification in brachytherapy based on time resolved in vivo dosimetry. Phys Med 2019;60:156–61. https://doi.org/10.1016/j.ejmp.2019.03.031.
[23] Jørgensen EB, Buus S, Bentzen L, Hokland SB, Rylander S, Kertzscher G, et al. 3D dose reconstruction based on in vivo dosimetry for determining the dosimetric impact of geometric variations in high-dose-rate prostate brachytherapy. Radiother Oncol 2022. https://doi.org/10.1016/j.radonc.2022.01.006.
[24] Kertzscher G, Beddar S. Inorganic scintillation detectors for 192Ir brachytherapy. Phys Med Biol 2019;64:225018. https://doi.org/10.1088/1361-6560/ab421f.
[25] Westerveld H, Nesvacil N, Fokdal L, Chargari C, Schmid MP, Milosevic M, et al. Definitive radiotherapy with image-guided adaptive brachytherapy for primary vaginal cancer. Lancet Oncol 2020;21:e157–67. https://doi.org/10.1016/S1470-2045(19)30855-1.
[26] Schmid MP, Fokdal L, Westerveld H, Chargari C, Rohl L, Morice P, et al. Recommendations from gynaecological (GYN) GEC-ESTRO working group - ACROP: target concept for image guided adaptive brachytherapy in primary vaginal cancer. Radiother Oncol 2020;145:36–44. https://doi.org/10.1016/j.radonc.2019.11.005.
[27] Jørgensen EB, Johansen JG, Overgaard J, Piché-Meunier D, Tho D, Rosales HML, et al. A high-Z inorganic scintillator–based detector for time-resolved in vivo dosimetry during brachytherapy. Med Phys 2021;48:7382–98. https://doi.org/10.1002/mp.15257.
[28] Andreo P, Burns DT, Hohlfeld K, Huq Saiful M, Kanai T, Laitano F, et al. Absorbed dose determination in external beam radiotherapy: an international code of practice for dosimetry based on standards of absorbed dose to water: TRS-398. Int At Energy Agency 2000.
[29] Kaveckyte V, Jørgensen EB, Kertzscher G, Johansen JG, Carlsson TÅ. Monte Carlo characterization of high atomic number inorganic scintillators for in vivo dosimetry in 192Ir brachytherapy. Med Phys 2022;49:4715–30. https://doi.org/10.1002/mp.15674.
[30] Meigooni AS, Meli JA, Nath R. Influence of the variation of energy spectra with depth in the dosimetry of 192Ir using LiF TLD. Phys Med Biol 1988;33:1159. https://doi.org/10.1088/0031-9155/33/10/005.
[31] Georgi PD, Jørgensen EB, Heidotting M, Tanderup K, Kertzscher G, Graversen JJ. A simple calibration routine for small inorganic scintillation detectors for in vivo dosimetry during brachytherapy. Brachytherapy 2024.
[32] Jørgensen EB, Kertzscher G, Buus S, Bentzen L, Hokland SB, Rylander S, et al. Accuracy of an in vivo dosimetry-based source tracking method for afterloading brachytherapy — a phantom study. Med Phys 2021;48:2614–23. https://doi.org/10.1002/mp.14812.
[33] Perez-Calatayud J, Ballester F, Das RK, DeWerd LA, Ibbott GS, Meigooni AS, et al. Dose calculation for photon-emitting brachytherapy sources with average energy higher than 50 keV: report of the AAPM and ESTRO. Med Phys 2012;39:2904–29. https://doi.org/10.1118/1.3703892.
[34] Miften M, Olch A, Mihailidis D, Moran J, Pawlicki T, Molineu A, et al. Tolerance limits and methodologies for IMRT measurement-based verification QA: Recommendations of AAPM Task Group No. 218. Med Phys 2018;45:e53–83. https://doi.org/10.1002/mp.12810.
[35] van Wagenberg T, Paiva Fonseca G, Voncken R, van Beveren C, van Limbergen E, Lutgens L, et al. Treatment verification in high dose rate brachytherapy using a realistic 3D printed head phantom and an imaging panel. Brachytherapy 2023. https://doi.org/10.1016/j.brachy.2022.11.012.
[36] Mohamed Yoosuf AB, Jeevanandam P, Whitten G, Workman G, McGarry CK. Verification of high-dose-rate brachytherapy treatment planning dose distribution using liquid-filled ionization chamber array. J Contemp Brachytherapy 2018;10:142–54. https://doi.org/10.5114/jcb.2018.75599.
[37] Buus S, Lizondo M, Hokland S, Rylander S, Pedersen EM, Tanderup K, et al. Needle migration and dosimetric impact in high-dose-rate brachytherapy for prostate cancer evaluated by repeated MRI. Brachytherapy 2018;17:50–8. https://doi.org/10.1016/j.brachy.2017.08.005.